

Fine-grained topological structures hidden in Fermi sea

Wei Jia^{1,*}

¹Key Laboratory of Quantum Theory and Applications of MoE, Lanzhou Center for Theoretical Physics, and Key Laboratory of Theoretical Physics of Gansu Province, Lanzhou University, Lanzhou 730000, China
(Dated: March 20, 2026)

The geometry of Fermi sea hosts a unique form of quantum topology that governs the conductance quantization of metal and is characterized by the Euler characteristic χ_F , offering a new perspective in the study of topological quantum matter. Here, we discover that characterizing Fermi sea topology solely by χ_F is insufficient: Fermi seas with identical χ_F can exhibit fundamentally different fine-grained topological structures that cannot be connected without a Lifshitz transition. To encode this hidden structure, we introduce a structural resolution factor that captures the fine-grained Fermi sea topologies beyond χ_F . Considering the attractive Hubbard interaction of electrons on Fermi surfaces, we further demonstrate that the resulting topological superconducting phases can inherit the fine-grained Fermi sea topology of their normal filled bands, with differences in these structures giving rise to anomalous gapless boundary states at the interface between two metal-superconductor heterojunctions. This work opens an avenue for understanding the topological richness of Fermi sea.

Introduction. Quantum topology is a cornerstone of modern condensed matter physics that has reshaped our understanding of electronic phases and material properties [1–5]. A most prominent example is topological phases, whose quantum topology arises from the global feature of wave function across the Brillouin zone (BZ), determined by defining topological invariant of the ground state [6–8]. The well-established topological classification has provided a solid foundation for understanding such nontrivial phases [9–14]. However, in a metallic system, there is another quantum topology dictated by the geometry of Fermi sea, which significantly impacts the quantized response of the system [15–18]. The resulting conductance quantization has been observed in quantum point contacts [19], semiconductor nanowires [20, 21], and carbon nanotubes [22]. Despite its long-standing importance, a fundamental understanding of Fermi sea topology has remained elusive.

Very recently, a breakthrough has elucidated that the Fermi sea topology is characterized by the Euler characteristic χ_F [23]. This characterization reveals that two Fermi seas with the same χ_F are topologically equivalent, as one can be smoothly deformed into the other without crossing a Lifshitz transition (LT) [24]. With this theoretical framework, various probing schemes for χ_F have been proposed, including multipartite entanglement [25], Andreev state transport [26, 27], and density correlations of Fermi gas [28–30]. The quantized response may also be possible to measured in an ultracold atomic gas [31–33]. Moreover, when an attractive Hubbard interaction of electrons on Fermi surfaces (FSs) are considered, the metal can become topological superconductor [34–37], of which the topological invariants of superconducting (SC) states are related to χ_F of parent filled bands [38, 39]. Nevertheless, a fundamental question remains: does χ_F alone provide a complete description of Fermi sea topology, particularly when contrasted with the exhaustive classification of topological phases?

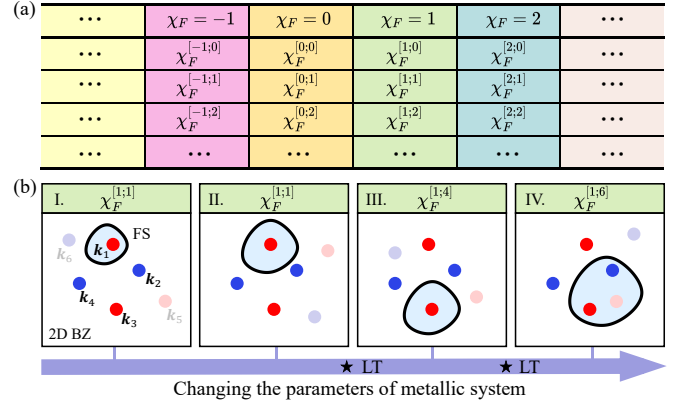


FIG. 1. (a) The redefined $\chi_F^{[w+v;g]}$ provides a comprehensive description of Fermi sea topology, where $w+v$ gives the Euler characteristic, but the structural resolution factor g determines its fine-grained topological structures. (b) A schematic to calculate $\chi_F^{[w+v;g]}$ for four different Fermi seas. Here $\mathbf{k}_{1,2,\dots,6}$ are critical points hosting $\eta_{1,3,5} = 1$ and $\eta_{2,4,6} = -1$, where $\mathbf{k}_{1,2,3,4}$ are the FCPs and $\mathbf{k}_{5,6}$ are the ACPs. The fine-grained topological structures of I (II), III, and IV are markedly different.

In this Letter, we demonstrate that the Euler characteristic χ_F is insufficient to fully characterize Fermi sea topology. Specifically, we show that the two-dimensional (2D) Fermi seas with identical χ_F can host distinct fine-grained topological structures that cannot be connected without passing through a LT, revealing a layer of topological information beyond the reach of χ_F . To capture this fine structure, we introduce a structural resolution factor, establishing a complete and universal framework to describe the Fermi sea topology. We further show that topological SC phases emerging from attractive Hubbard interactions of electrons on FSs can inherit the fine-grained topology of their parent metallic bands. Particularly, the differences in these structures give rise to anomalous gapless boundary states at interfaces be-

tween metal-superconductor heterojunctions. Our work not only refines the theoretical understanding of Fermi sea topology but also provides an insight for exploring the topological richness within the Fermi sea.

Fine-grained Fermi sea topology. Our starting point is a 2D metallic system featuring the electronic band $E_{\mathbf{k}}$ in momentum space. The Fermi sea in such a system gives rise to a novel quantum topology characterized by the Euler characteristic χ_F , which governs its quantization of nonlinear conductance [23]. The Morse theory [40, 41] provides to calculate χ_F through

$$\chi_F = \sum_m \eta_m. \quad (1)$$

Here m labels the critical points \mathbf{k}_m within the Fermi sea, where $\mathbf{v}_{\mathbf{k}} = \nabla_{\mathbf{k}} E_{\mathbf{k}} = 0$ and $E_{\mathbf{k}} < E_F$. For convenience, we take the Fermi level E_F as zero energy. The signature of each critical point is given by $\eta_m = \text{sgn}[\det(\mathbb{H})]$, where \mathbb{H} is Hessian matrix of $E_{\mathbf{k}}$. Note that \mathbf{k}_m are considered as nondegenerate, i.e., $\det(\mathbb{H}) \neq 0$. When a critical point passes through E_F , it allows χ_F change at a LT. Under this theoretical framework, two Fermi seas are topologically equivalent provided one can be smoothly deformed into the other without crossing a LT, since they share the same χ_F . Nevertheless, if the deformation involves LTs that change the number and position of \mathbf{k}_m , these two Fermi seas may differ in their fine-grained topological structures even through χ_F remains unchanged. This fine-grained topology clearly extends beyond the description provided by χ_F .

To exactly capture the fine-grained topological structures of Fermi sea, we firstly assume that, in addition to having M critical points in the Fermi sea, there are also N critical points that are not within it. All the critical points are denoted as $\mathbf{k}_1, \mathbf{k}_2, \dots, \mathbf{k}_Q, \dots, \mathbf{k}_{M+N}$. When the parameters of system are adjusted, the positions of certain critical points in the BZ remain unchanged, while others may shift. These can be dubbed as fixed critical points (FCPs) and adjustable critical points (ACPs), respectively. We adopt a unified index that $i = 1, \dots, Q$ are for the FCPs and $i = Q + 1, \dots, M + N$ are for the ACPs. Secondly, we introduce another signature

$$\varepsilon_i = \text{sgn}(E_{\mathbf{k}_i} - E_F) \quad (2)$$

for each \mathbf{k}_i , where $\varepsilon_i = 1$ (-1) describes \mathbf{k}_i be located at the outside (inside) of Fermi sea. By defining $\kappa_i = \eta_i \varepsilon_i$ to characterize the overall signature of \mathbf{k}_i , the topological properties of FCPs and ACPs can be determined by the \mathbb{Z} -classified topological indexes w and v , respectively. The explicit expressions are given by

$$w = -\frac{1}{2} \sum_{i=1}^Q \kappa_i, \quad v = -\frac{1}{2} \sum_{i=Q+1}^{M+N} \kappa_i. \quad (3)$$

Furthermore, the LTs that keep the Euler characteristic unchanged have two classes: those driven solely by

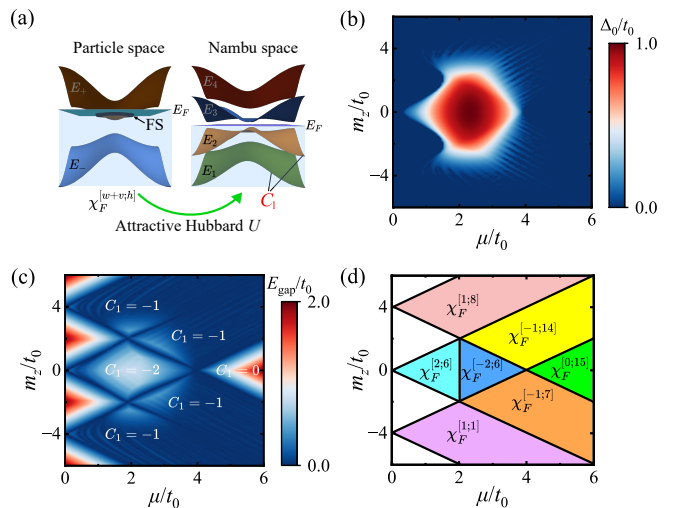


FIG. 2. (a) Chiral topological SC phases are induced by considering an attractive Hubbard interaction of electrons on the FS. (b)-(c) Self-consistent calculations of the pairing order for (b) and the SC bulk gap for (c) at zero temperature. (d) Phase diagram indicated by $\chi_F^{[w+v;g]}$, where there are four FCPs $\mathbf{k}_i = \mathbf{A}_i = \{\mathbf{M}, \mathbf{X}_1, \mathbf{X}_2, \mathbf{\Gamma}\}$ with $i = 1, 2, 3, 4$. In white regions, the system is an insulator phase. The other parameters are $t_{so} = t_0$ and $U = 5t_0$.

FCPs crossing E_F , and those driven by FCPs and ACPs crossing E_F simultaneously. And then, one can define a structural resolution factor

$$g = \sum_{i=1}^Q 2^{(i-1)} \gamma_i \quad (4)$$

to determine the sequence properties of $\{\varepsilon_i\}$ for all the FCPs, where $(-1)^{\gamma_i} = \varepsilon_i$. Finally, the Euler characteristic can be redefined as

$$\chi_F^{[w+v;g]} = w + v, \quad (5)$$

where $g \in \mathbb{N}$ characterizes the fine-grained topological structures of Fermi sea. It is clear that $\chi_F^{[w+v;g]}$ provides a comprehensive description of the 2D Fermi sea topology, as shown in Fig. 1(a). We further show a schematic diagram to illustrate how $\chi_F^{[w+v;g]}$ work, as shown in Fig. 1(b). By changing the parameters of system, the Fermi sea of case I can be sequentially deformed into the cases II, III, and IV. The fine-grained topological structures of Fermi sea are markedly different for the cases I (II), III, and IV, even though they share the same Euler characteristic. Hence this theory provides a universal framework to characterize the fine-grained topological structures of Fermi sea [42].

Interaction-induced superconducting phases. For a 2D metallic system, the electrons on FSs can produce Cooper pairs under an attractive Hubbard interaction, resulting in the emergence of SC phases [43–47]. Accordingly, the

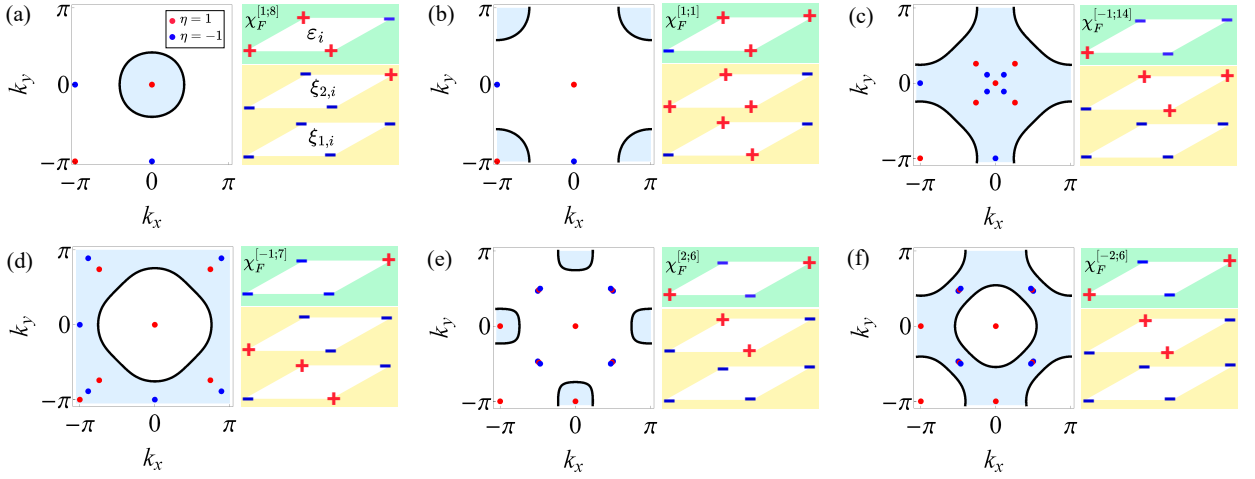


FIG. 3. The different configurations of Fermi seas (left) and the signs of ε_i and $\xi_{j,i}$ at the FCPs $\mathbf{k}_i = \mathbf{\Lambda}_i$ (right). For the chiral topological SC phases, we have $(C_1; g_1, g_2) = (-1; 15, 7)$, $(-1; 9, 8)$, $(-1; 15, 1)$, $(-1; 9, 14)$, $(-2; 15, 9)$, and $(-2; 15, 9)$ for (a)-(f), respectively. The parameters of (m_z, μ, Δ_0) are taken as $(3t_0, 2t_0, 0.249t_0)$ for (a), $(-3t_0, 2t_0, 0.249t_0)$ for (b), $(2.1t_0, 3t_0, 0.4103t_0)$ for (c), $(-2.1t_0, 3t_0, 0.4103t_0)$ for (d), $(0.2t_0, 1.5t_0, 0.7912t_0)$ for (e), and $(0.2t_0, 2.5t_0, 0.9834t_0)$ for (f), respectively. The other parameters are $t_{\text{so}} = t_0$ and $U = 5t_0$.

SC properties can be greatly affected by the fine-grained Fermi sea topology of their normally filled bands. Here, we consider a family of 2D metallic bands with

$$E_{\pm} = \pm \sqrt{h_{1,\mathbf{k}}^2 + h_{2,\mathbf{k}}^2 + h_{3,\mathbf{k}}^2} - \mu, \quad (6)$$

which are from the Hamiltonian $H_0 = \sum_{\mathbf{k}} \psi_{\mathbf{k}}^{\dagger} H_{\mathbf{k}} \psi_{\mathbf{k}}$ with $H_{\mathbf{k}} = h_{1,\mathbf{k}} \sigma_x + h_{2,\mathbf{k}} \sigma_y + h_{3,\mathbf{k}} \sigma_z - \mu$. Here $\psi_{\mathbf{k}} = (c_{\mathbf{k},\uparrow}, c_{\mathbf{k},\downarrow})$ is the spinor in particle space and μ is the chemical potential. By taking a reasonable parameter for μ , the metallic phases emerge, where the upper band E_+ is partially or completely filled. Next, we introduce the attractive Hubbard interaction with the strength U into this metallic system. The SC phases are induced by $U > 0$, as shown in Fig. 2(a). The total Hamiltonian is written as $\mathcal{H}_{\mathbf{k}} = H_0 - U \sum_i n_{i\uparrow} n_{i\downarrow}$, where $n_{i\sigma} = c_{i\sigma}^{\dagger} c_{i\sigma}$ is the particle number operator. The possible pairing order is considered as $\Delta_0 = \frac{U}{2P} \sum_{\mathbf{k}} \langle c_{\mathbf{k}\uparrow} c_{-\mathbf{k}\downarrow} \rangle$, with zero center-of-mass momentum of Cooper pairs and P being number of sites. Under the mean field approach, the interaction term is decoupled into $H_U = \sum_{\mathbf{k}} \Delta_0 c_{\mathbf{k}\uparrow}^{\dagger} c_{-\mathbf{k}\downarrow}^{\dagger} + \text{h.c.}$ and $\mathcal{H}_{\mathbf{k}}$ can be rewritten as

$$\mathcal{H}_{\text{MF}} = \frac{1}{2} \sum_{\mathbf{k}} \Psi_{\mathbf{k}}^{\dagger} H_{\text{MF}} \Psi_{\mathbf{k}}, \quad H_{\text{MF}} = \begin{pmatrix} H_{\mathbf{k}} & \Delta \\ \Delta^{\dagger} & -H_{-\mathbf{k}}^{\text{T}} \end{pmatrix}, \quad (7)$$

where $\Delta = i\Delta_0 \sigma_y$ and the basis is denoted as $\Psi_{\mathbf{k}} = (c_{\mathbf{k},\uparrow}, c_{\mathbf{k},\downarrow}, c_{-\mathbf{k},\uparrow}^{\dagger}, c_{-\mathbf{k},\downarrow}^{\dagger})$ in Nambu space. Here, we take $h_{1,\mathbf{k}} = 2t_{\text{SO}} \sin k_x \cos k_y$, $h_{2,\mathbf{k}} = 2t_{\text{SO}} \sin k_y$, and $h_{3,\mathbf{k}} = [m_z - 2t_0 (\cos k_x + \cos k_y)]$, where m_z is the Zeeman constant, t_0 (t_{SO}) is the coefficient of spin-conserved (spin-flipped) hopping, and $\sigma_{x,y,z}$ are the Pauli matrices on spin space. By taking $\mu = 0$, the Hamiltonian $H_{\mathbf{k}}$ shows an effective low-energy model driving quantum anomalous Hall states, and then \mathcal{H}_{MF} can render the 2D chiral

topological SC phases [34, 35, 43]. We therefore expect that the properties of chiral topological SC phases can be effected by the fine-grained Fermi sea topology of their normally filled bands.

After choosing an interaction as $U = 5t_0$ and performing the self-consistent calculations, we numerically obtain the pairing order in Fig. 2(b) and the SC bulk gap in Fig. 2(c), of which the Chern number C_1 is calculated by the TKNN number [48–50] and is confirmed by the spectrum of Wannier charge center [51–53]. The details are provided in the Supplementary Material [42]. We observe that the SC bulk gap closes at four high-symmetric momentum points $\mathbf{\Lambda}_i = \{\mathbf{M}, \mathbf{X}_1, \mathbf{X}_2, \mathbf{\Gamma}\}$ for $\Delta_0^2 + \mu^2 = (m_z - 4t_0)^2$, m_z^2 , and $(m_z + 4t_0)^2$, respectively. It is surprised that there are bulk gap closing to distinguish two topological SC phases with the same Chern number, as shown in Fig. 2(c). This result implies that these two SC phases have the difference in fine-grained topological structures, and thus they cannot be connected through the deformations that do not close the bulk gap. By calculating the redefined Euler characteristic of normally filled bands and showing it in Fig. 2(d), we demonstrate that the above results are closely associated with the fine-grained Fermi sea topology of their normally filled bands. Namely, the difference of structural resolution factor g in Fermi sea determines the emergence of topological phase transitions of SC phases. For instance of $m_z > 0$, the SC phases with $C_1 = -1$ are in the regions of $\chi_F^{[1;8]}$ and $\chi_F^{[-1;14]}$, holding the different g . Thus the bulk gap closing appear in these two SC phases. In contrast, there is no bulk gap closing for the SC phases with $C_1 = -2$, since their normally filled bands give $\chi_F^{[2;6]}$ and $\chi_F^{[-2;6]}$ which share the same g .

The above results reveal a fundamental physical mechanism, i.e., the interaction-induced SC phases can inherit the fine-grained Fermi sea topology of their normally filled bands. The reason is that the parity eigenvalues $\xi_{j,i}$ at four high-symmetric points $\mathbf{\Lambda}_i$ for the two occupied bands $E_{j,\mathbf{k}}$ in the SC phases are related to the structural resolution factor of FCPs, where $j = 1, 2$. Considering that the SC system has inversion symmetry $\mathcal{I} = \tau_z \sigma_z$, where $\boldsymbol{\tau}$ are Pauli matrices acting on the Nambu space, the parities of these two occupied bands satisfy

$$\varepsilon_i = \prod_{j=1,2} \xi_{j,i}. \quad (8)$$

We provide six configurations of Fermi seas in Fig. 3, which are taken in the different phase regions of Fig. 2(d). It is clear that ε_i and $\xi_{j,i}$ at the FCPs $\mathbf{k}_i = \mathbf{\Lambda}_i$ obey the Eq. (8). With this, one can define two structural resolution factors $g_j = \sum_{i=1}^Q 2^{(i-1)\gamma_{j,i}}$ with $j = 1, 2$ to describe the fine-grained topological structures of the chiral topological SC phases, where $(-1)^{\gamma_{j,i}} = \xi_{j,i}$ and $Q = 4$. And then, the topological indexes $(C_1; g_1, g_2)$ characterize the chiral topological SC phases, as shown in Fig. 3. This scheme effectively distinguishes two same topological SC phases that have different fine-grained topological structures [42]. It should be noted that the Eq. (8) drives $\gamma_i = \gamma_{1,i} \oplus \gamma_{2,i}$ and

$$g = g_1 \oplus g_2, \quad (9)$$

where \oplus is an exclusive OR function with the properties of $A \oplus 0 = A$, $A \oplus A = 0$, and $A \oplus B = B \oplus A$. This implies that two interaction-induced topological SC phase have the different g_j , when their normally filled bands host the different g . Hence, the Eq. (9) directly confirms that the fine-grained Fermi sea topology can be inherited by the topological SC phases.

Anomalous gapless interface states. For chiral topological insulators or chiral topological superconductors, the gapless states can appear at the interface between topologically distinct systems and manifest as chiral modes, when changing the topological invariants [54–56]. Especially for two distinct 2D systems, the number of chiral modes at the interface is determined by $N_{\text{chiral}} = |C_{1,L} - C_{1,R}|$ [57–60], where $C_{1,L}$ and $C_{1,R}$ are the Chern numbers of left-hand and right-hand topological systems, respectively. Hence there is a fact that no gapless states appear at the interface when $C_{1,L} = C_{1,R}$. However, we hereby show an anomalous phenomenon, i.e., two gapless states with opposite chirality can emerge in the interface of two metal-superconductor heterojunctions (MSCHs) with the same Chern numbers. This result is associated with the difference of fine-grained Fermi sea topologies of two metals in the MSCHs.

Specifically, each MSCH is produced by putting a metal on the surface of a superconductor, as shown in Fig. 4. If the band dispersion of the metal is given by

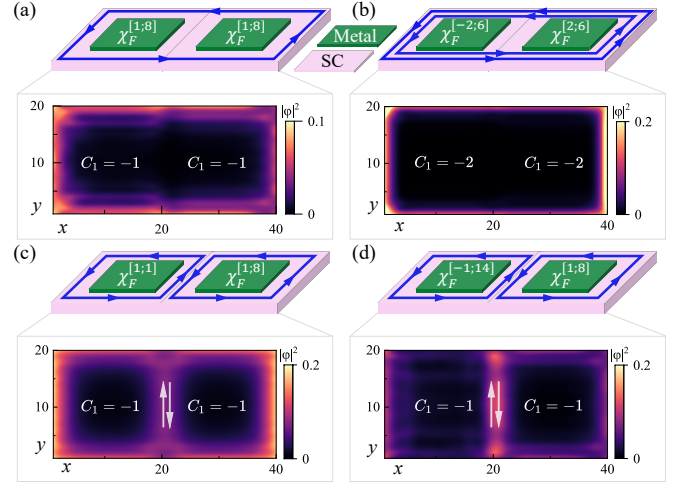


FIG. 4. Two connected metal-superconductor heterojunctions without (a)-(b) and with anomalous gapless interface states (c)-(d), where the insets are the real-space distributions of 40 states near zero energy. The Chern numbers of these chiral topological SC phases are $C_{1,L} = C_{1,R} = -1$ for (a), (c), (d), and $C_{1,L} = C_{1,R} = -2$ for (b). We take $(m_{z,L}, \mu_L, m_{z,R}, \mu_R) = (3t_0, 2.5t_0, 3t_0, 2t_0)$ for (a), $(0.2t_0, 1.5t_0, 0.2t_0, 2.5t_0)$ for (b), $(-3t_0, 2t_0, 3t_0, 2t_0)$ for (c), and $(2.1t_0, 3t_0, 3t_0, 2t_0)$ for (d), respectively. The other parameters are $t_{so} = t_0$ and $U = 5t_0$.

Eq. (6) obeying $H_{\mathbf{k}}$, the MSCH can support the chiral topological SC phases and described by \mathcal{H}_{MF} [43]. When two metals in the connected MSCHs have different fine-grained Fermi sea topology, two topological SC phases have different structural resolution factors and cannot smoothly deform into each other, even though having the same Chern number. Accordingly, the gapless states shall inevitably appear at the interface of two connected MSCHs. Here, we take the Fermi sea topologies of two metals as $\chi_F^{[1;8]}$, as shown in Fig. 4(a). Both interaction-induced topological SC phases exhibit $(C_1; g_1, g_2) = (-1; 15, 7)$. Hence there is no gapless states at the interface of two connected MSCHs. The similar results are also observed by changing two metals into $\chi_F^{[-2;6]}$ and $\chi_F^{[2;6]}$, where two topological SC phases have $(C_1; g_1, g_2) = (-2; 15, 9)$, as shown in Fig. 4(b).

When separately choosing $\chi_F^{[1;1]}$ and $\chi_F^{[1;8]}$ for two metals, the different fine-grained structures of Fermi sea topology lead to $(C_1; g_1, g_2) = (-1; 9, 8)$ and $(-1; 15, 7)$ for the left-hand and right-hand MSCH, respectively. Even though two topological SC phases still host the same C_1 , the gapless states emerge at the interface of two MSCHs due to the difference of $g_{1,2}$, as shown in Fig. 4(c). The similar results are also found in Fig. 4(d), where the Fermi sea topology of two metals are $\chi_F^{[-1;14]}$ and $\chi_F^{[1;8]}$. The two topological SC phases have $(C_1; g_1, g_2) = (-1; 15, 1)$ and $(-1; 15, 7)$ for the left-hand and right-hand MSCH, respectively. These results demonstrate

that the fine-grained topological structures of Fermi sea can bring the novel physical phenomena.

Conclusion. We have demonstrated that the metallic systems can host fine-grained topological structures in their Fermi seas, which extends beyond the description provided by the Euler characteristic. Also, we have proposed a structural resolution factor to effectively characterize them. Such fine-grained Fermi sea topology can induce several novel physical phenomena: (i) the Fermi seas with matching Euler characteristics but differing structural resolution factors cannot be adiabatically connected; (ii) the interaction-induced superconducting phases inherit the fine-grained Fermi sea topology of parent filled bands, imprinting it onto the topology of pairing states; (iii) the differences of fine-grained Fermi sea topology induce anomalous gapless states in the interface two connected metal-superconductor heterojunctions. These nontrivial results establish a new paradigm for understanding the intricate topology of Fermi sea.

Acknowledgements. We thank Long Zhang for helpful discussions. This work is supported by the National Natural Science Foundation of China (Grant No. 12404318 and No. 12247101), the Fundamental Research Funds for the Central Universities (Grant No. lzujbky-2024-jdzz06), the Natural Science Foundation of Gansu Province (No. 22JR5RA389 and No. 25JRRA799).

* jiaw@lzu.edu.cn

- [1] K. v. Klitzing, G. Dorda, and M. Pepper, New method for high-accuracy determination of the fine-structure constant based on quantized Hall resistance, *Phys. Rev. Lett.* **45**, 494 (1980).
- [2] D. C. Tsui, H. L. Stormer, and A. C. Gossard, Two-dimensional magnetotransport in the extreme quantum limit, *Phys. Rev. Lett.* **48**, 1559 (1982).
- [3] M. Z. Hasan and C. L. Kane, Colloquium: topological insulators, *Rev. Mod. Phys.* **82**, 3045 (2010).
- [4] X.-L. Qi and S.-C. Zhang, Topological insulators and superconductors, *Rev. Mod. Phys.* **83**, 1057 (2011).
- [5] X.-G. Wen, Colloquium: Zoo of quantum-topological phases of matter, *Rev. Mod. Phys.* **89**, 041004 (2017).
- [6] R. B. Laughlin, Quantized Hall conductivity in two dimensions, *Phys. Rev. B* **23**, 5632 (1981).
- [7] D. J. Thouless, M. Kohmoto, M. P. Nightingale, and M. den Nijs, Quantized hall conductance in a two-dimensional periodic potential, *Phys. Rev. Lett.* **49**, 405 (1982).
- [8] C.-K. Chiu, J. C. Y. Teo, A. P. Schnyder, and S. Ryu, Classification of topological quantum matter with symmetries, *Rev. Mod. Phys.* **88**, 035005 (2016).
- [9] A. Kitaev, Periodic table for topological insulators and superconductors, *AIP Conf. Proc.* **1134**, 22 (2009).
- [10] L. Fidkowski and A. Kitaev, Topological phases of fermions in one dimension, *Phys. Rev. B* **83**, 075103 (2011).
- [11] L. Fu, Topological crystalline insulators, *Phys. Rev. Lett.* **106**, 106802 (2011).
- [12] T. Morimoto and A. Furusaki, Topological classification with additional symmetries from Clifford algebras, *Phys. Rev. B* **88**, 125129 (2013).
- [13] K. Shiozaki and M. Sato, Topology of crystalline insulators and superconductors, *Phys. Rev. B* **90**, 165114 (2014).
- [14] Y. Ren, Z. Qiao, and Q. Niu, Topological phases in two-dimensional materials: a review, *Reports on Progress in Physics* **79**, 066501 (2016).
- [15] R. Landauer, Spatial variation of currents and fields due to localized scatterers in metallic conduction, *IBM J. Res. Dev.* **1**, 223 (1957).
- [16] D. S. Fisher and P. A. Lee, Relation between conductivity and transmission matrix, *Phys. Rev. B* **23**, 6851 (1981).
- [17] M. Büttiker, Four-terminal phase-coherent conductance, *Phys. Rev. Lett.* **57**, 1761 (1986).
- [18] A. D. Stone and A. Szafer, What is measured when you measure a resistance?—The Landauer formula revisited, *IBM J. Res. Dev.* **32**, 384 (1988).
- [19] B. J. Van Wees, H. Van Houten, C. W. J. Beenakker, J. G. Williamson, L. P. Kouwenhoven, D. Van der Marel, and C. T. Foxon, Quantized conductance of point contacts in a two-dimensional electron gas, *Phys. Rev. Lett.* **60**, 848 (1988).
- [20] T. Honda, S. Tarucha, T. Saku, and Y. T. Y. Tokura, Quantized conductance observed in quantum wires 2 to 10 μm long, *Jpn. J. Appl. Phys.* **34**, L72 (1995).
- [21] I. van Weperen, S. R. Plissard, E. P. Bakkers, S. M. Frolov, and L. P. Kouwenhoven, Quantized conductance in an insb nanowire, *Nano Lett.* **13**, 387 (2013).
- [22] S. Frank, P. Poncharal, Z. Wang, and W. A. d. Heer, Carbon nanotube quantum resistors, *Science* **280**, 1744 (1998).
- [23] C. Kane, Quantized nonlinear conductance in ballistic metals, *Phys. Rev. Lett.* **128**, 076801 (2022).
- [24] I. M. Lifshitz, Anomalies of electron characteristics of a metal in the high pressure region, *Sov. Phys. JETP* **11**, 1130 (1960).
- [25] P. M. Tam, M. Claassen, and C. L. Kane, Topological multipartite entanglement in a Fermi liquid, *Phys. Rev. X* **12**, 031022 (2022).
- [26] P. M. Tam and C. L. Kane, Probing Fermi sea topology by Andreev state transport, *Phys. Rev. Lett.* **130**, 096301 (2023).
- [27] P. M. Tam, C. De Beule, and C. L. Kane, Topological andreev rectification, *Phys. Rev. B* **107**, 245422 (2023).
- [28] P. M. Tam and C. L. Kane, Topological density correlations in a Fermi gas, *Phys. Rev. B* **109**, 035413 (2024).
- [29] C. Daix, P. M. Tam, M. Dixmierias, J. Verstraten, T. de Jongh, B. Peaudecerf, C. L. Kane, and T. Yef-sah, Probing the fermi sea topology in a quantum gas, [arXiv:2511.23353](https://arxiv.org/abs/2511.23353) (2025).
- [30] P. M. Tam and C. L. Kane, Singular three-point density correlations in two-dimensional fermi liquids, [arXiv:2602.16774](https://arxiv.org/abs/2602.16774) (2026).
- [31] F. Yang and H. Zhai, Quantized nonlinear transport with ultracold atoms, *Quantum* **6**, 857 (2022).
- [32] P. Zhang, Quantized topological response in trapped quantum gases, *Phys. Rev. A* **107**, L031305 (2023).
- [33] F. Yang and X. Li, Quantized nonlinear transport and its breakdown in fermi gases with berry curvature, *Phys. Rev. B* **113**, 075431 (2026).
- [34] L. Fu and C. L. Kane, Superconducting proximity effect and majorana fermions at the surface of a topological

- insulator, *Phys. Rev. Lett.* **100**, 096407 (2008).
- [35] X.-J. Liu, K. T. Law, and T. K. Ng, Realization of 2D spin-orbit interaction and exotic topological orders in cold atoms, *Phys. Rev. Lett.* **112**, 086401 (2014).
- [36] T. F. J. Poon and X.-J. Liu, From a semimetal to a chiral fulde-ferrell superfluid, *Phys. Rev. B* **97**, 020501 (2018).
- [37] W. Jia, Z.-H. Huang, X. Wei, Q. Zhao, and X.-J. Liu, Topological superfluids for spin-orbit coupled ultracold fermi gases, *Phys. Rev. B* **99**, 094520 (2019).
- [38] F. Yang, X. Li, and C. Li, Euler-Chern correspondence via topological superconductivity, *Phys. Rev. Research* **5**, 033073 (2023).
- [39] W. Jia, Generic reduction theory for fermi sea topology in metallic systems, *Phys. Rev. B* **111**, 155115 (2025).
- [40] J. W. Milnor, *Morse theory*, Vol. 51 (Princeton University Press, 1963).
- [41] C. Nash and S. Sen, *Topology and geometry for physicists* (Elsevier, 1988).
- [42] See Supplemental Material for the details.
- [43] X.-L. Qi, T. L. Hughes, and S.-C. Zhang, Chiral topological superconductor from the quantum hall state, *Phys. Rev. B* **82**, 184516 (2010).
- [44] S. B. Chung, H.-J. Zhang, X.-L. Qi, and S.-C. Zhang, Topological superconducting phase and majorana fermions in half-metal/superconductor heterostructures, *Phys. Rev. B* **84**, 060510 (2011).
- [45] B. A. Bernevig, *Topological insulators and topological superconductors* (Princeton university press, 2013).
- [46] M. Sato and Y. Ando, Topological superconductors: a review, *Rep. Prog. Phys.* **80**, 076501 (2017).
- [47] C. Chan, L. Zhang, T. F. J. Poon, Y.-P. He, Y.-Q. Wang, and X.-J. Liu, Generic theory for majorana zero modes in 2d superconductors, *Phys. Rev. Lett.* **119**, 047001 (2017).
- [48] Y. Hatsugai, Chern number and edge states in the integer quantum hall effect, *Phys. Rev. Lett.* **71**, 3697 (1993).
- [49] M. Sato and S. Fujimoto, Topological phases of noncentrosymmetric superconductors: Edge states, majorana fermions, and non-abelian statistics, *Phys. Rev. B* **79**, 094504 (2009).
- [50] X.-L. Qi, Y.-S. Wu, and S.-C. Zhang, General theorem relating the bulk topological number to edge states in two-dimensional insulators, *Phys. Rev. B* **74**, 045125 (2006).
- [51] A. A. Soluyanov and D. Vanderbilt, Wannier representation of F_2 topological insulators, *Phys. Rev. B* **83**, 035108 (2011).
- [52] M. Taherinejad, K. F. Garrity, and D. Vanderbilt, Wannier center sheets in topological insulators, *Phys. Rev. B* **89**, 115102 (2014).
- [53] W. A. Benalcazar, B. A. Bernevig, and T. L. Hughes, Electric multipole moments, topological multipole moment pumping, and chiral hinge states in crystalline insulators, *Phys. Rev. B* **96**, 245115 (2017).
- [54] I. T. Rosen, E. J. Fox, X. Kou, L. Pan, K. L. Wang, and D. Goldhaber-Gordon, Chiral transport along magnetic domain walls in the quantum anomalous hall effect, *npj Quantum Materials* **2**, 69 (2017).
- [55] Y.-F. Zhao, R. Zhang, J. Cai, D. Zhuo, L.-J. Zhou, Z.-J. Yan, M. H. Chan, X. Xu, and C.-Z. Chang, Creation of chiral interface channels for quantized transport in magnetic topological insulator multilayer heterostructures, *Nat. Comm.* **14**, 770 (2023).
- [56] C. Zhang, T. Zhu, S. Kahn, T. Soejima, K. Watanabe, T. Taniguchi, A. Zettl, F. Wang, M. P. Zaletel, and M. F. Crommie, Manipulation of chiral interface states in a moiré quantum anomalous hall insulator, *Nat. Phys.* **20**, 951 (2024).
- [57] M. Liu, W. Wang, A. R. Richardella, A. Kandala, J. Li, A. Yazdani, N. Samarth, and N. P. Ong, Large discrete jumps observed in the transition between chern states in a ferromagnetic topological insulator, *Sci. Adv.* **2**, e1600167 (2016).
- [58] Y. Wan, J. Li, and Q. Liu, Topological magnetoelectric response in ferromagnetic axion insulators, *Nat. Sci. Rev.* **11**, nwac138 (2024).
- [59] Q. Yan, H. Li, H. Jiang, Q.-F. Sun, and X. Xie, Rules for dissipationless topotronics, *Sci. Adv.* **10**, eado4756 (2024).
- [60] Y.-H. Wan, P.-Y. Liu, and Q.-F. Sun, Classification of chern numbers based on high-symmetry points, *Phys. Rev. B* **111**, L161410 (2025).

Supplementary Material for “Fine-grained topological structures hidden in Fermi sea”

In this Supplementary Material, we provide the details of the fine-grained Fermi sea topology and the properties of chiral topological superconducting phases. Besides, more numerical results are also provided.

I. More instructions of fine-grained Fermi sea topology

Our theory can apply to the more generic 2D metallic system with n filled bands, i.e., $E_{j,\mathbf{k}}$ with $j = 1, 2, \dots, n$, where only one top band $E_{n,\mathbf{k}}$ crosses Fermi level $E_F = 0$. This top band is denoted as $E_{\mathbf{k}}$ and is used to determine the Fermi sea topology, since all the completely filled bands in the below of E_F exhibit $\chi_F = 0$. Furthermore, one can define a quantity

$$G_{\mathbf{k}} = \sqrt{E_{\mathbf{k}}^2 + \mathbf{v}_{\mathbf{k}}^2} \quad (\text{S1})$$

and find $G = \min[G_{\mathbf{k}}] = 0$ if there is a LT. And then, the certain fixed critical points (FCPs) are located at Fermi surfaces (FSs), giving a solution of \mathbf{k} for $E_{\mathbf{k}} = \mathbf{v}_{\mathbf{k}} = 0$. Besides, it should be noted that the metallic bands generally possess some symmetries, and thus the positions of FCPs in Brillouin zone (BZ) are unchanged when the parameters of system are adjusted. This case requires $E_{\mathbf{k}}$ be an odd or even function of k_i , where i takes several or all directions of momenta.

We next consider a 2D typical metallic band $E_{\mathbf{k}}$, which is neither an odd nor an even function of \mathbf{k} , i.e., $E_{\mathbf{k}} \neq E_{-\mathbf{k}} \neq -E_{-\mathbf{k}}$. The corresponding band dispersion is given by

$$E_{\mathbf{k}} = t_0 + t_0 \sin k_y + t_1 \cos k_x \sin k_y + t_2 \cos k_x \cos 2k_y. \quad (\text{S2})$$

Nevertheless, one can find $E_{\mathbf{k}}$ is a even function of k_x , i.e., $E_{k_x, k_y} = E_{-k_x, k_y}$, and thus there are four FCPs $\mathbf{k}_1 = (-\pi, -\pi/2)$, $\mathbf{k}_2 = (-\pi, \pi/2)$, $\mathbf{k}_3 = (0, -\pi/2)$, and $\mathbf{k}_4 = (0, \pi/2)$ in the BZ. We numerically obtain G in Fig. S1(a) and the configurations of Fermi seas in Fig. S1(b). It is seen that two Fermi seas with the same Euler characteristics are clearly separated by one LT or several LTs. This implies that these two Fermi seas host the different fine-grained topological structures, determined by the different structural resolution factor g . For instance of two Fermi seas with $\chi_F^{[1;1]}$ and $\chi_F^{[1;4]}$, when we change the Fermi sea topology from $\chi_F^{[1;1]}$ into $\chi_F^{[1;4]}$, the signature of η of \mathbf{k}_2 (\mathbf{k}_4) is changed from $\eta_2 = -1$ ($\eta_4 = 1$) into $\eta_2 = 1$ ($\eta_4 = -1$). The signature of ε of \mathbf{k}_1 (\mathbf{k}_3) is changed from $\varepsilon_2 = -1$ ($\varepsilon_3 = 1$) into $\varepsilon_2 = 1$ ($\varepsilon_3 = -1$). Correspondingly, g is changed from $g = 1$ into $g = 4$, giving the different fine-grained Fermi sea topology. These results further show that the redefined Euler characteristic $\chi_F^{[w+v;g]}$ can effectively characterize the comprehensive topology of Fermi sea.

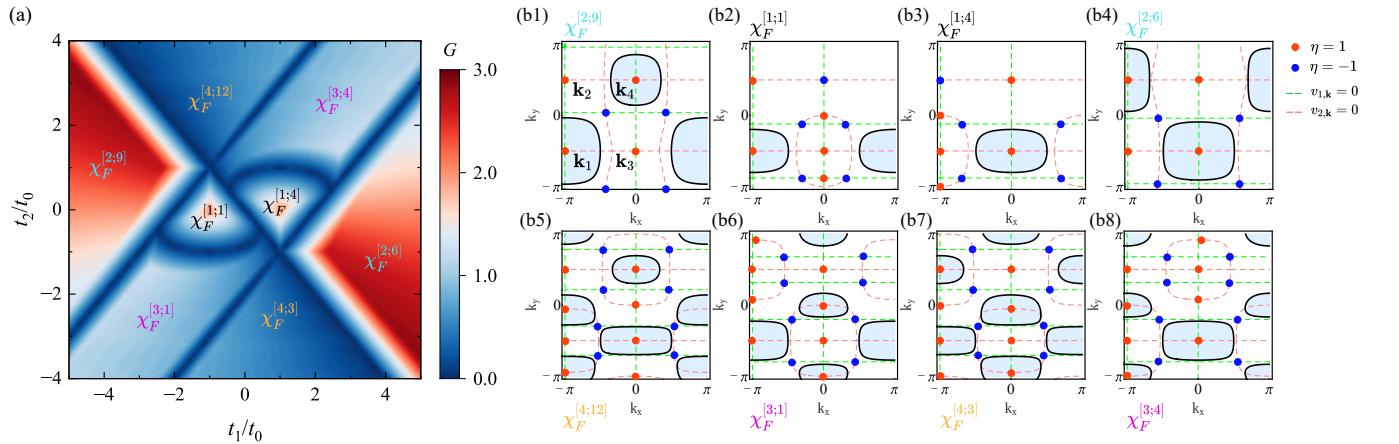


FIG. S1. The numerical results of G for (a) and the different Fermi sea structures for (b). The black curves give the Fermi surfaces (FSs) and the lightblue regions denote the insides of Fermi seas with $E_{\mathbf{k}} < 0$. The green and red dashed lines give $v_{1,\mathbf{k}} = 0$ and $v_{2,\mathbf{k}} = 0$, respectively. The critical points are captured by $v_{1,\mathbf{k}} = v_{2,\mathbf{k}} = 0$, where the FCPs are \mathbf{k}_1 , \mathbf{k}_2 , \mathbf{k}_3 , and \mathbf{k}_4 , and the others are the ACPs. Here the parameters of (t_1, t_2) are taken as $(-4t_0, 0.5t_0)$ for $\chi_F^{[2;9]}$, $(-t_0, 0.5t_0)$ for $\chi_F^{[1;1]}$, $(t_0, 0.5t_0)$ for $\chi_F^{[1;4]}$, $(4t_0, 0.5t_0)$ for $\chi_F^{[2;6]}$, $(-t_0, 2t_0)$ for $\chi_F^{[4;12]}$, $(-t_0, -3t_0)$ for $\chi_F^{[3;1]}$, $(t_0, -2t_0)$ for $\chi_F^{[4;3]}$, and $(t_0, 3t_0)$ for $\chi_F^{[3;4]}$, respectively.

II. More properties of chiral topological superconducting phases

For the 2D chiral topological superconducting (SC) phases induced by attractive Hubbard interaction in metallic bands, the mean-field Hamiltonian H_{MF} is written as

$$H_{\text{MF}} = \begin{pmatrix} H_{\mathbf{k}} & \Delta \\ \Delta^\dagger & -H_{-\mathbf{k}}^T \end{pmatrix}, \quad (\text{S3})$$

where we have chosen $H_{\mathbf{k}} = h_{1,\mathbf{k}}\sigma_x + h_{2,\mathbf{k}}\sigma_y + h_{3,\mathbf{k}}\sigma_z - \mu$ and $\Delta = i\Delta_0\sigma_y$. Here three h components are taken as $h_{1,\mathbf{k}} = 2t_{\text{SO}} \sin k_x \cos k_y$, $h_{2,\mathbf{k}} = 2t_{\text{SO}} \sin k_y$, and $h_{3,\mathbf{k}} = [m_z - 2t_0(\cos k_x + \cos k_y)]$. It is noted that the bulk gap of H_{MF} is closing at four high-symmetric momentum points \mathbf{M} , $\mathbf{X}_{1,2}$, and Γ , when the parameters satisfy $\Delta_0^2 + \mu^2 = (m_z - 4t_0)^2$, m_z^2 , and $(m_z + 4t_0)^2$, respectively. The corresponding results are shown in Fig. S2(a). Generally, the topological phase transition caused by the band gap closing is accompanied by a change in the topological number. However, here we emphasize that the difference of fine-grained topology can induce the band gap closing even though two topological SC phases share the same topological number. The main reason is that the topological SC phases inherit the fine-grained Fermi sea topology of their normally filled bands. And then, the SC phases are characterized

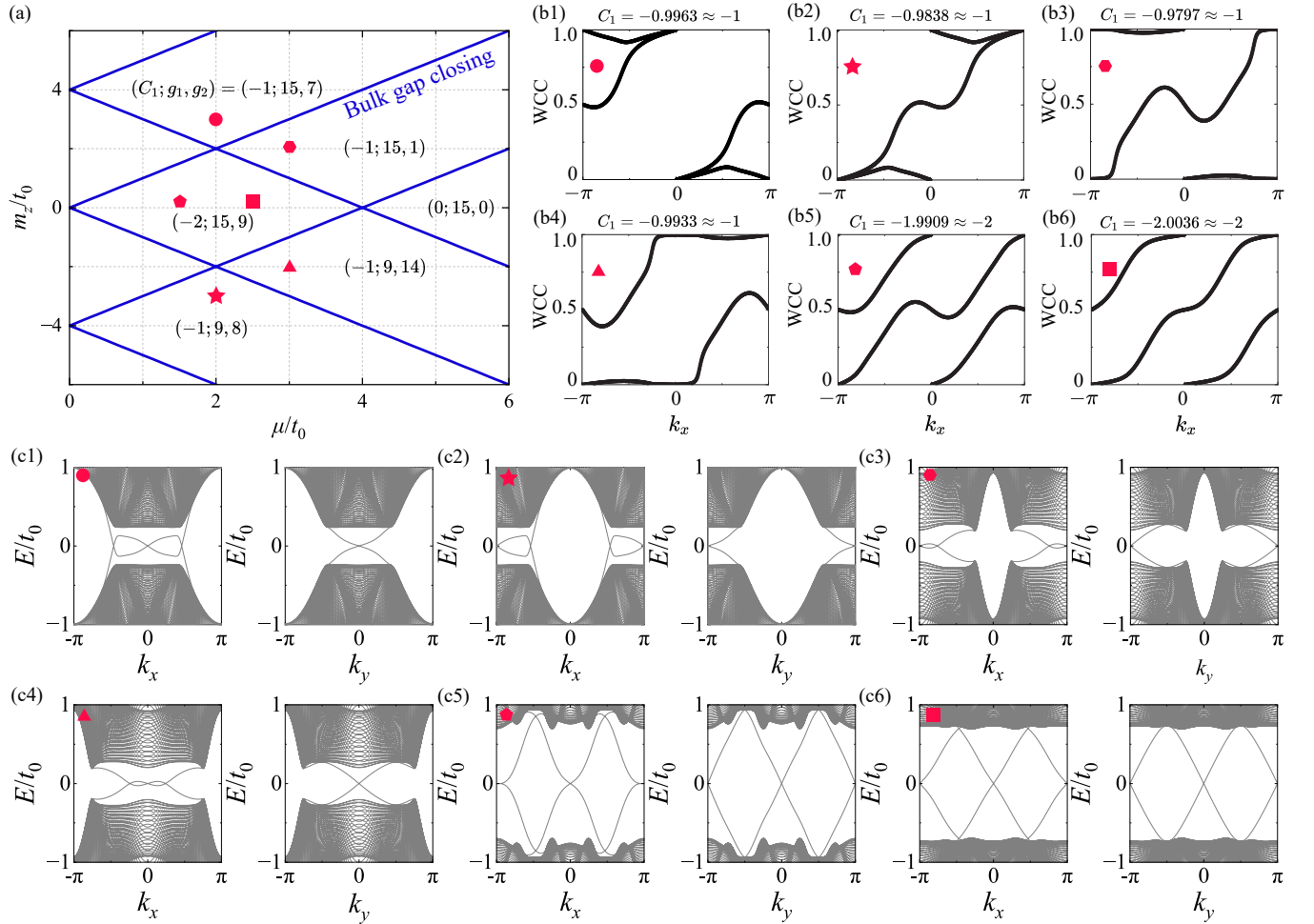


FIG. S2. (a) The phase diagram determined by $(C_1; g_1, g_2)$. (b1)-(b6) The numerical results of C_1 and the spectra of WCC, where the parameters are taken as $(m_z, \mu, \Delta_0) = (3t_0, 2t_0, 0.249t_0)$ for (b1), $(-3t_0, 2t_0, 0.249t_0)$ for (b2), $(2.1t_0, 3t_0, 0.4103t_0)$ for (b3), $(-2.1t_0, 3t_0, 0.4103t_0)$ for (b4), $(0.2t_0, 1.5t_0, 0.7912t_0)$ for (b5), and $(0.2t_0, 2.5t_0, 0.9834t_0)$ for (b6). The energy spectra of k_x or k_y open boundary conditions correspond to the (b1)-(b6). The other parameters are $t_{\text{SO}} = t_0$ and $U = 5t_0$.

by $(C_1; g_1, g_2)$, as shown in Fig. S2(a). The Chern number C_1 of two occupied bands is calculated by

$$C_1 = -\frac{1}{2\pi} \iint_{\text{BZ}} dk_x dk_y \text{Im} \sum_{a=1}^2 \sum_{b=3}^4 \frac{\langle u_a | \partial_{k_x} H_{\text{MF}} | u_b \rangle \langle u_b | \partial_{k_y} H_{\text{MF}} | u_a \rangle - \langle u_a | \partial_{k_y} H_{\text{MF}} | u_b \rangle \langle u_b | \partial_{k_x} H_{\text{MF}} | u_a \rangle}{(E_a - E_b)^2}, \quad (\text{S4})$$

where $H_{\text{MF}} |u_j\rangle = E_j |u_j\rangle$ with $j = 1, 2, 3, 4$. Moreover, the Chern number C_1 is further confirmed by the spectra of Wannier charge center (WCC), as shown in Fig. S2(b). The topological phases with $C_1 = -1$ (-2) clearly drive a winding number $W = -1$ (-2) of WCC spectrum. Finally, the spectra of H_{MF} under k_x or k_y open boundary conditions are provided in Fig. S2(c), showing the difference of edge states for the same chiral topological SC phases. Since we generalize the characterization framework of the fine-grained Fermi sea topology into the fine-grained topological structures of SC phases, this demonstrates the universality of this theory.